

## Superconducting NbSe<sub>2</sub> nanowires and nanoribbons converted from NbSe<sub>3</sub> nanostructures

Y. S. Hor, U. Welp, Y. Ito,<sup>a)</sup> Z. L. Xiao,<sup>a),b)</sup> U. Patel,<sup>a)</sup> J. F. Mitchell,  
W. K. Kwok, and G. W. Crabtree

Materials Science Division, Argonne National Laboratory, Argonne, Illinois 60439

(Received 18 May 2005; accepted 22 August 2005; published online 27 September 2005)

We describe the synthesis of superconducting NbSe<sub>2</sub> nanowires and nanoribbons by the nondestructive removal of Se from one-dimensional NbSe<sub>3</sub> nanostructure precursors. We report scanning electron microscopy imaging, x-ray diffraction, and transmission electron microscopy analyses of the morphology, composition, and crystallinity of the converted NbSe<sub>2</sub> nanostructures. Transport measurements on individual nanowires/ribbons confirm their superconductivity with  $T_c \sim 7.2$  K, and the appearance of current-induced resistance steps is attributed to localized phase slip centers, akin to those reported in other superconducting nanostructures. © 2005 American Institute of Physics. [DOI: 10.1063/1.2072847]

One-dimensional (1D) nanostructures in the form of wires, ribbons, and tubes have received steadily growing attention due to their unusual properties and application potentials which are superior to their bulk counterparts.<sup>1</sup> Due to the confinement of Cooper pairs and supercurrent flows, new phenomena, such as quantum phase slips<sup>2-4</sup> and quantum switch effects,<sup>5</sup> are expected to appear in 1D superconductors. Furthermore, 1D superconducting nanostructures are also highly desirable in future nanodevices as electrical connections. Numerous efforts have been made to synthesize superconducting nanostructures.<sup>6-14</sup> The most common approach is to use nanochannels in porous membranes as templates to form metal nanowires of Pb (Refs. 6-8) and Sn (Refs. 8 and 9) through electrodeposition. Other methods include the fabrication of MoGe (Refs. 3 and 4) and Nb (Ref. 10) nanowires by sputtering them onto bridges of carbon nanotubes. Progress has also been made in synthesizing Pb nanowires by thermal decomposition of lead acetate in ethylene glycol (Ref. 11) and directly growing Pb nanowires onto graphite substrates at high electrodeposition reduction potentials.<sup>12</sup> Superconducting nanowires of MgB<sub>2</sub> have also been fabricated by annealing B nanowires in Mg vapors.<sup>13,14</sup>

Superconducting NbSe<sub>2</sub> crystals have been used in recent years as a model system to study vortex dynamics.<sup>15-18</sup> Therefore, it is of interest to pursue the physics of confinement effects in 1D superconducting NbSe<sub>2</sub> nanostructures. Furthermore, superconducting NbSe<sub>2</sub> nanostructures are far more stable at ambient atmosphere than oxophilic Pb, Sn, and Nb nanostructures, thus avoiding problems of surface oxidation that are normally encountered in metal nanowires.

NbSe<sub>2</sub> nanotubes and nanorods were observed when sintering NbSe<sub>3</sub> powders under inert gas flow, and NbSe<sub>2</sub> nanowires were also obtained through a solution-based synthesis approach.<sup>19,20</sup> The NbSe<sub>2</sub> nanostructures synthesized with these methods are quite small (a few nm to tens of nm in diameters). Vortex confinement studies in superconductors require the sample cross section to be comparable with the penetration depth (230 nm at zero temperature and increases with increasing temperature). Recently, we developed a con-

venient and controllable way to synthesize monocrystalline NbSe<sub>3</sub> nanowires and nanoribbons.<sup>21</sup> Here, we report the synthesis and characterization of a new class of 1D superconductors — NbSe<sub>2</sub> nanowires and nanoribbons by the transformation of NbSe<sub>3</sub> nanostructures. Their transverse dimensions range from about 10 nanometers to submicrometers. The synthesized NbSe<sub>2</sub> nanoribbons can provide a new platform for pursuing novel confinement phenomena, such as “few vortex rows” physics<sup>22</sup> in 1D superconductors.

Crucial to this conversion process is the balance of two competing reactions. On the one hand, the removal of Se from NbSe<sub>3</sub> occurs at high temperatures, but on the other hand, these high temperatures can lead to the destruction of the nanostructures. Annealing NbSe<sub>3</sub> in flowing inert gas above 300 °C caused selenium to bleach out of the NbSe<sub>3</sub>.<sup>19</sup> However, there is no convenient way to monitor the composition change during annealing NbSe<sub>3</sub>. Therefore, it is difficult to control the conversion of NbSe<sub>3</sub> into NbSe<sub>2</sub> nanowires with this approach. In fact, we typically obtained nanowires and nanoribbons of NbO<sub>x</sub> when annealing NbSe<sub>3</sub> nanostructures in flowing argon or nitrogen atmospheres, probably due to the unavoidable residual oxygen in the argon gas or to oxygen outgassing from the quartz tube itself.

The controlled conversion from NbSe<sub>3</sub> into NbSe<sub>2</sub> nanostructures was realized in an evacuated quartz tube containing a stoichiometric proportion of NbSe<sub>3</sub> nanostructures and Nb powder which satisfied the chemical equilibrium reaction  $2\text{NbSe}_2 + \text{Nb} \leftrightarrow 3\text{NbSe}_3$ . Upon heating, the selenium bleaches out of NbSe<sub>3</sub> and is absorbed by the Nb powder. The bleaching automatically terminates once the Nb powder is completely consumed. In experiments, we placed NbSe<sub>3</sub> nanostructures<sup>21</sup> on one end of the quartz tube and a stoichiometric amount of Nb powder at the center of the tube, approximately 5 cm away from the NbSe<sub>3</sub> nanostructures. The tube was evacuated and purged repeatedly with ultrahigh-purity argon gas. The ampoule was then sealed under a vacuum and heated up to a fixed temperature at the rate of 3 °C/min, held at a temperature for various times, and then cooled down at 2 °C/min to room temperature.

We found that a temperature between 600 °C and 700 °C enabled the conversion from NbSe<sub>3</sub> to NbSe<sub>2</sub> while preserving the shapes of the NbSe<sub>3</sub> nanostructures. Figure 1 depicts the x-ray diffraction (XRD) patterns of the NbSe<sub>3</sub> nanostruc-

<sup>a)</sup>Also at: Department of Physics, Northern Illinois University, DeKalb, IL 60115.

<sup>b)</sup>Electronic mail: xiao@anl.gov or zxiao@niu.edu

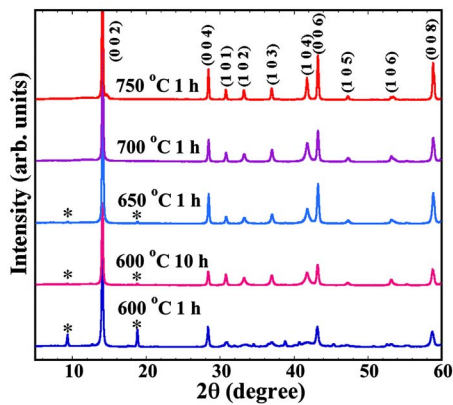


FIG. 1. (Color online) XRD patterns of the resultants from annealing  $\text{NbSe}_3$  nanostructures in sealed quartz tubes with an appropriate amount of Nb powder at various temperatures. The indexed peaks are for the  $\text{NbSe}_2$  phase, while the asterisks mark the remaining  $\text{NbSe}_3$  phase.

tures after annealing for various annealing times at 600 °C, 650 °C, 700 °C, and 750 °C. It is evident that the  $\text{NbSe}_3$  phase is converted into the  $\text{NbSe}_2$  phase. The trace appearance of  $\text{NbSe}_3$  in samples annealed at low temperatures, e.g., 600 °C, is understandable if the conversion of  $\text{NbSe}_3$  to  $\text{NbSe}_2$  starts at the surface of the  $\text{NbSe}_3$  nanostructures. During the conversion, a superconducting  $\text{NbSe}_2$  shell forms on the surface and propagates inward with a rate that is strongly temperature dependent. At low temperatures, it takes a long time to achieve a complete conversion. This is probably the reason why the  $\text{NbSe}_3$  phase still exists in samples annealed for 10 h at 600 °C, while it completely disappears in samples obtained at 700 °C for only 1 h. In fact, a 20 min (the shortest time we tried) annealing at 700 °C led to the complete conversion of  $\text{NbSe}_3$  to  $\text{NbSe}_2$ .

We used scanning electron microscopy (SEM) to image the nanostructures before and after annealing. Figure 2 shows typical SEM images of the converted  $\text{NbSe}_2$  nanostructures. Wires and ribbons of various sizes can be seen. The highest temperature for preserving the shapes of  $\text{NbSe}_3$  nanostructures is about 700 °C. At higher temperatures, microrods and platelike structures can be observed. This maximum temperature coincides with the decomposition temperature of  $\text{NbSe}_3$ .<sup>21</sup> However, it can also be the decomposition temperature of  $\text{NbSe}_2$  nanostructures, though bulk  $\text{NbSe}_2$  decomposes at 840 °C.<sup>23</sup> According to the above discussions on the conversion at low temperatures,  $\text{NbSe}_2$  shells should start to form on  $\text{NbSe}_3$  wires at 600 °C. It takes about 30 min to ramp up to 700 °C with the applied ramping rate of

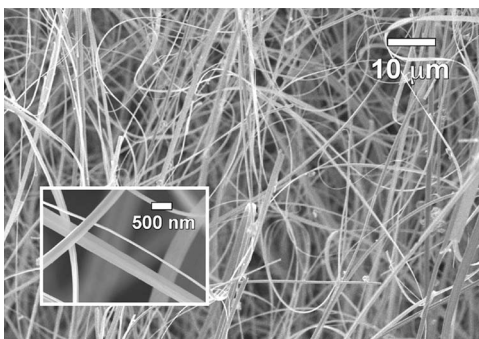


FIG. 2. SEM micrographs of the converted  $\text{NbSe}_2$  nanostructures through Se-reduction of  $\text{NbSe}_3$  nanostructures at 600 °C for 10 h. The high magnification image given in the inset shows the varieties in size and in shape of the nanostructures.

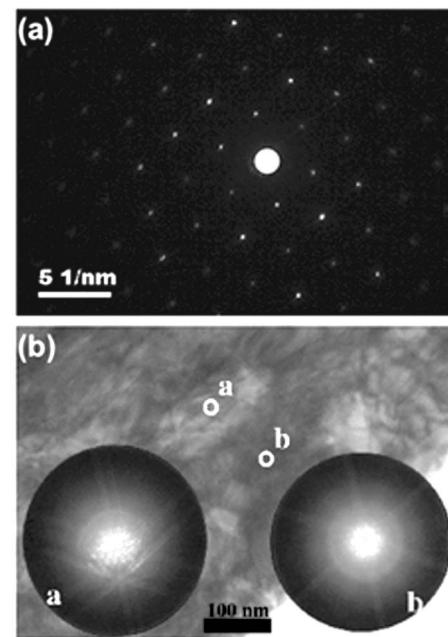


FIG. 3. SAED pattern (a) and TEM image (b) of a  $\text{NbSe}_2$  nanoribbon. Insets of (b) show the CBED patterns and Kikuchi lines at locations denoted with letters a and b. The two sets of hexagonal diffraction patterns and Kikuchi lines observed at location a reveal the misorientation along the thickness direction.

3 °C/min. Therefore,  $\text{NbSe}_2$  shells should be thick enough to maintain the shapes of the  $\text{NbSe}_3$  nanostructures after  $\text{NbSe}_3$  cores decompose at 700 °C. A lower decomposition temperature of the converted  $\text{NbSe}_2$  nanostructure can be caused by a high density of defects, such as dislocations and/or grain boundaries, which can appear because the atoms have to adjust their positions during the conversion. Although nearly perfect patterns, as shown in Fig. 3(a), were observed in the selected area electron diffractions (SAEDs), we did find a high density of grain boundaries through high-resolution transmission electron microscopy (TEM) imaging. The convergent beam electron diffraction (CBED) patterns and Kikuchi lines, as shown in the insets of Fig. 3(b) also identify the existence of misoriented microcrystallines with respect to the background along the thickness direction, e.g., in the area a of the nanoribbon. We found similar microcrystallines distributed throughout the sample.

A superconducting quantum interference device magnetometer was used to characterize the superconductivity of the converted  $\text{NbSe}_2$  nanostructures (in an amount of mg). The critical temperature ( $T_c$ ) for samples annealed at temperatures of 630 °C and above, was found to be close to 7.2 K, the typical value for bulk samples. For samples which show a small percentage of  $\text{NbSe}_3$  phase in the XRD patterns,  $T_c$  decreases with increasing amount of  $\text{NbSe}_3$ . This can be considered as indirect evidence of the formation of the  $\text{NbSe}_2/\text{NbSe}_3$  shell/core structure which leads to lower  $T_c$  due to the proximity effect.

Transport measurements were conducted to investigate the superconductivity of individual nanowires. The inset of Fig. 4(a) shows a  $\text{NbSe}_2$  nanowire with two gold contacts. The applied magnetic field is perpendicular to the plane. Figure 4(a) shows the temperature dependence of resistance at various applied magnetic fields. The critical temperature of this single  $\text{NbSe}_2$  nanowire is 7.05 K at zero field. From these resistance versus temperature curves, one can deter-

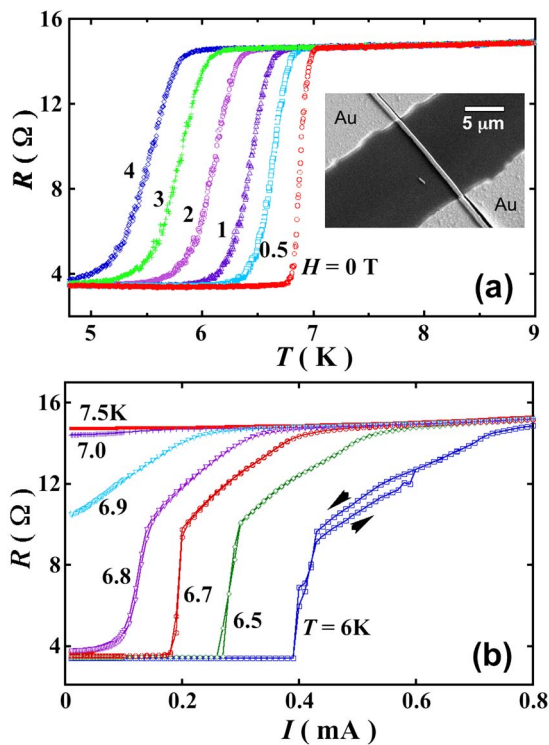


FIG. 4. (Color online) (a) Temperature dependence of the resistance of a 800 nm wide NbSe<sub>2</sub> nanowire in various magnetic fields. The inset shows the two-probe construction of the resistance measurement. Two gold pads (brighter areas) are separated by a 12.5 μm gap (darker area). (b) Resistance,  $R$ , as a function of applied current,  $I$ , at various temperatures. The arrows indicate the current sweep directions.

mine a magnetic-field versus temperature phase diagram of the normal and superconducting states. This diagram (not shown) gives a value of 4.2 T/K for  $dH_c/dT$ , which is larger by a factor of 6 and 2, in comparison with the bulk values in the  $c$  direction and  $a$ - $b$  plane,<sup>24</sup> respectively. It is predicted that the critical field  $H_c^*$  is larger than the bulk value of  $H_c$  for a superconductor with a dimension of the order of the effective penetration depth  $\lambda_e$ . Such an enhancement of the critical field in small samples results from the reduced free-energy density of the superconducting state due to the more significant effect of the field penetration. For a long cylindrical mesowire, the theoretically predicted relationship between  $H_c^*$  and  $H_c$  is  $H_c^*/H_c = 8\lambda_e/d$ , where  $d$  is the diameter of the mesowire. This has been confirmed in Pb nanowires.<sup>25</sup> For the measured NbSe<sub>2</sub> nanowire, a two-fold enhancement in the critical field compared to its bulk value in the  $a$ - $b$  plane is consistent with the prediction of a factor of 2.3, assuming that the field in our experiment is parallel to the  $a$ - $b$  plane and the penetration depth is 230 nm.<sup>24</sup>

One of the potential applications of 1D superconducting nanostructures is as interconnects in nanodevices. Therefore, the current-carrying capability of a nanostructure should be one of the important characterizations. Furthermore, fundamental parameters, such as quasiparticle diffusion length and inelastic scattering time can be deduced from transport studies at high dissipation levels.<sup>26</sup> This type of investigation has been carried out for most of the currently available superconducting nanowires by measuring the voltage-current ( $V$ - $I$ ) or resistance-current ( $R$ - $I$ ) characteristics. Voltage or resistance steps often appear at high currents and are usually interpreted to be induced by spatially localized phase-slip centers.<sup>7-10</sup> As

shown in Fig. 4(b), resistance steps also occur in the  $R$ - $I$  curves of the converted NbSe<sub>2</sub> nanowires.

In conclusion, we have successfully converted NbSe<sub>3</sub> nanowires and nanoribbons into superconducting NbSe<sub>2</sub> nanostructures through a controlled Se-reduction approach. The conversion takes place in the narrow reaction temperature range of 600 °C–700 °C. Both magnetization and transport measurements confirm the superconductivity of the converted NbSe<sub>2</sub> nanostructures, which have critical temperatures reaching the bulk value of 7.2 K. Confinement-induced enhancement of the critical fields and resistance steps in the  $R$ - $I$  characteristics were observed in the synthesized NbSe<sub>2</sub> superconducting nanowires and nanoribbons.

This work was supported by the US Department of Energy, BES-Materials Science, Contract no. W-31-109-ENG-38. One of the authors (Z. L. X) also acknowledges support from the U.S. Department of Education. The scanning/transmission electron microscopies were performed in the Electron Microscopy Center at Argonne.

<sup>1</sup>For a recent review, see Y. N. Xia, P. D. Yang, Y. G. Sun, Y. Y. Wu, B. Mayers, B. Gates, Y. D. Yin, F. Kim, and Y. Q. Yan, *Adv. Mater.* (Weinheim, Germany) **15**, 353 (2003).

<sup>2</sup>A. D. Zaikin, D. S. Golubev, A. van Otterlo, and G. T. Zimanyi, *Phys. Rev. Lett.* **78**, 1552 (1997).

<sup>3</sup>A. Bezryadin, C. N. Lau, and M. Tinkham, *Nature* (London) **404**, 971 (2000).

<sup>4</sup>C. N. Lau, N. Markovic, M. Bockrath, A. Bezryadin, and M. Tinkham, *Phys. Rev. Lett.* **87**, 217003 (2001).

<sup>5</sup>A. S. Mel'nikov and V. M. Vinokur, *Nature* (London) **415**, 60 (2002).

<sup>6</sup>G. Yi and W. Schwarzacher, *Appl. Phys. Lett.* **74**, 1746 (1999).

<sup>7</sup>D. Y. Vodolazov, F. M. Peeters, L. Piroux, S. Matefi-Tempfli, and S. Michotte, *Phys. Rev. Lett.* **91**, 157001 (2003).

<sup>8</sup>S. Michotte, S. Matefi-Tempfli, and L. Piroux, *Appl. Phys. Lett.* **82**, 4119 (2003).

<sup>9</sup>M. L. Tian, J. G. Wang, J. Snyder, J. Kurtz, Y. Liu, P. Schiffer, T. E. Mallouk, and M. H. W. Chan, *Appl. Phys. Lett.* **83**, 1620 (2003).

<sup>10</sup>A. Rogachev and A. Bezryadin, *Appl. Phys. Lett.* **83**, 512 (2003).

<sup>11</sup>Y. L. Wang, X. C. Jiang, T. Herricks, and Y. N. Xia, *J. Phys. Chem. B* **108**, 8631 (2004).

<sup>12</sup>Z. L. Xiao, C. Y. Han, W. K. Kwok, H. W. Wang, U. Welp, J. Wang, and G. W. Crabtree, *J. Am. Chem. Soc.* **126**, 2316 (2004).

<sup>13</sup>Y. Y. Wu, B. Messer, and P. D. Yang, *Adv. Mater.* (Weinheim, Germany) **13**, 1487 (2001).

<sup>14</sup>Q. Yang, J. Sha, X. Y. Ma, Y. J. Ji, and D. R. Yang, *Supercond. Sci. Technol.* **17**, L31 (2004).

<sup>15</sup>Z. L. Xiao, E. Y. Andrei, and M. J. Higgins, *Phys. Rev. Lett.* **83**, 1664 (1999).

<sup>16</sup>A. M. Troyanovski, J. Aarts, and P. H. Kes, *Nature* (London) **399**, 665 (1999).

<sup>17</sup>M. Marchevsky, M. J. Higgins, and S. Bhattacharya, *Nature* (London) **409**, 591 (2001).

<sup>18</sup>Y. Paltiel, E. Zeldov, Y. N. Myasoedov, H. Shtrikman, S. Bhattacharya, M. J. Higgins, Z. L. Xiao, E. Y. Andrei, P. L. Gammel, and D. J. Bishop, *Nature* (London) **403**, 398 (2000).

<sup>19</sup>M. Nath, S. Kar, A. K. Raychaudhuri, and C. N. R. Rao, *Chem. Phys. Lett.* **368**, 690 (2003).

<sup>20</sup>P. Sekar, E. C. Greyson, J. E. Barton, and T. W. Odom, *J. Am. Chem. Soc.* **127**, 2054 (2005).

<sup>21</sup>Y. S. Hor, Z. L. Xiao, U. Welp, Y. Ito, J. F. Mitchell, R. E. Cook, W. K. Kwok, and G. W. Crabtree, *Nano Lett.* **5**, 397 (2005).

<sup>22</sup>J. J. Palacios, *Phys. Rev. B* **57**, 10873 (1998).

<sup>23</sup>Alfa AESAR, Materials Safety Data Sheet, Product Code 13101 (1983).

<sup>24</sup>M. J. Higgins and S. Bhattacharya, *Physica C* **257**, 232 (1996).

<sup>25</sup>S. Dubois, A. Michel, J. P. Eymery, J. L. Duvail, and L. Piroux, *J. Mater. Res.* **14**, 665 (1999).

<sup>26</sup>W. J. Skocpol, M. R. Beasley, and M. Tinkham, *J. Low Temp. Phys.* **16**, 145 (1974).